NEOPLASIA
www.neoplasia.com

Volume 11 Number 8 August 2009 pp. 812–822 812

# Increased Plasma Colloid Osmotic Pressure Facilitates the Uptake of Therapeutic Macromolecules in a Xenograft Tumor Model[1]

**Matthias Hofmann*,†,2, Emmet McCormack‡,2, Maja Mujić‡, Maila Roßberg*, August Bernd*, Jürgen Bereiter-Hahn§, Bjørn Tore Gjertsen‡, Helge Wiig† and Stefan Kippenberger***

*Department of Dermatology and Venerology, Goethe-University, D-60590 Frankfurt/Main, Germany; †Department of Biomedicine, Section of Physiology, University of Bergen, N-5009 Bergen, Norway; ‡Institute of Medicine, Haematology Section, University of Bergen, and Department of Internal Medicine, Haematology Section, Haukeland University Hospital, N-5021 Bergen, Norway; §Kinematic Cell Research Group, Department of Cell Biology and Neurosciences, Goethe-University, D-60439 Frankfurt/Main, Germany

## Abstract

Elevated tumor interstitial fluid pressure (TIFP) is a characteristic of most solid tumors. Clinically, TIFP may hamper the uptake of chemotherapeutic drugs into the tumor tissue reducing their therapeutic efficacy. In this study, a means of modulating TIFP to increase the flux of macromolecules into tumor tissue is presented, which is based on the rationale that elevated plasma colloid osmotic pressure (COP) pulls water from tumor interstitium lowering the TIFP. Concentrated human serum albumin (20% HSA), used as an agent to enhance COP, reduced the TIFP time-dependently from 8 to 2 mm Hg in human tumor xenograft models bearing A431 epidermoid vulva carcinomas. To evaluate whether this reduction facilitates the uptake of macromolecules, the intratumoral distribution of fluorescently conjugated dextrans (2.5 mg/ml) and cetuximab (2.0 mg/ml) was probed using novel time domain near-infrared fluorescence imaging. This method permitted discrimination and semiquantification of tumor-accumulated conjugate from background and unspecific probe fluorescence. The coadministration of 20% HSA together with either dextrans or cetuximab was found to lower the TIFP significantly and increase the concentration of the substances within the tumor tissue in comparison to control tumors. Furthermore, combined administration of 20% HSA plus cetuximab reduced the tumor growth significantly in comparison to standard cetuximab treatment. These data demonstrate that increased COP lowers the TIFP within hours and increases the uptake of therapeutic macromolecules into the tumor interstitium leading to reduced tumor growth. This model represents a novel approach to facilitate the delivery of therapeutics into tumor tissue, particularly monoclonal antibodies.

*Neoplasia (2009) 11, 812–822*

## Introduction

Great efforts have been made to increase the specificity of targeted therapeutics in the fight against cancer; there are, however, barriers that limit uptake in the desired tumor site [1]. The central protagonist that counteracts the enrichment of pharmacological compounds within solid tumors is their enhanced tumor interstitial fluid pressure (TIFP).

Originally, in 1950, Young et al. [2] hypothesized that hydrostatic pressures in tumor interstitium were elevated. However, it was approximately 30 years before others and we demonstrated that the interstitial

Address all correspondence to: Matthias Hofmann, PhD, Department of Dermatology and Venerology, Goethe-University, Theodor-Stern Kai 7, D-60590 Frankfurt/Main, Germany. E-mail: Matthias.Hofmann@em.uni-frankfurt.de

[1]This research was supported by a Marie Curie Fellowship of the European Union (to M.H.), Dr. August Scheidel Stiftung (to M.H.), Volkswagenstiftung (I/80949 to M.H.), Deutsche Forschungsgemeinschaft (KI834/2-1 to S.K.), The Norwegian Cancer Society, The Research Council of Norway, EU 6th framework program Integrated Project "Angiotargeting" Contract no 504743 (to H.W.), and The Western Norway Regional Health Authority grants (911388 and 911182 to E.M.).

[2]These authors contributed equally to this work.

Received 20 April 2009; Revised 20 April 2009; Accepted 6 May 2009



DOI 10.1593/neo.09662

fluid pressures (IFP) in tumors were indeed increased [3,4]. Later, it has been shown that a high TIFP is a general property of solid tumors in experimental animals and humans [5]. Following these observations, it has been suggested that this increase in TIFP acts as a barrier against the efficient transvascular transport of therapeutics into tumors [6,7]. In normal tissue, the IFP has a value of −2 to 0 mm Hg, which is in stark contrast to the IFP in solid human or experimental tumors that can reach values between 3 and 40 mm Hg [8]. The origin of TIFP is mainly attributed to lymph-vessel abnormalities, abnormal vasculature, and the highly permeable blood vessel network in the tumor area [9–11]. In addition to these trigger factors, it is also assumed that increased contractility of fibroblasts in the tumor surrounding stroma plays a pivotal role in the development of high TIFP values [5]. Small molecules are much less affected by an enhanced TIFP, being primarily distributed through diffusional transport. However, macromolecules, such as monoclonal antibodies, accumulate through convectional transcapillary transport, which is counteracted by TIFP [1,5,11,12]. Thus, elevated TIFP is suggested to hamper the transfer of macromolecules such as monoclonal antibodies from the vascular system into the tumor interstitium surrounding the tumor cells [7,9]. Besides implications for tumor therapy, TIFP is also known to cause mechanical stress on the tumor capsule, a well-known trigger factor for cell proliferation [13,14].

In capillaries, *Starling Forces*, that is, the hydrostatic and colloid osmotic pressures (COPs) in capillaries and interstitium, regulate the net transcapillary filtration pressure [15]. In normal human capillaries, a high COP in the plasma tends to keep fluid in the vessels, whereas a high hydrostatic pressure in the capillaries together with a low COP and negative (or close to zero) IFP within the interstitium acts oppositely and results in fluid filtration into the interstitium, supporting tissue nutrition. In tumors, a high TIFP may counteract filtration and thus, delivery of therapeutic agents [5,16].

In the current work, in a xenograft tumor model, we tested the hypothesis whether an increase of the vascular COP by systemically administered human serum albumin (HSA) generates a fluid efflux from tumor tissue resulting in a decreased TIFP. Consecutively, the uptake of intravenously (IV) applied fluorescent-labeled macromolecular compounds (dextran or cetuximab) into the tumor tissue was measured. Data were obtained by fluorescence microscopy and novel-infrared, time domain optical imaging. Particularly, the latter allows semiquantification of the intratumoral substance accumulation. By using these methods, it was found that systemic application of concentrated HSA increases the uptake of macromolecules into solid tumors and delays tumor growth. This novel approach offers new perspectives for the application of macromolecular anticancer therapeutics.

## Materials and Methods

### *Drugs and Cells*

The A431 epidermoid vulva carcinoma cell line was purchased from the American Type Culture Collection (ATCC/LCSC Standards, Wesel, Germany) and was cultured in Dulbecco's modified Eagle's medium (Invitrogen, Karlsruhe, Germany) containing 10% fetal calf serum. Phosphorylation of p44/42 was detected using a phosphospecific antibody (Thr202/Tyr204; Cell Signaling Technology, Frankfurt/Main, Germany). Detection of total p44/42 (Cell Signaling Technology) served as a loading control.

TRITC-, Alexa488-, or Alexa680-labeled dextrans (40 kDa; Invitrogen) or Alexa680-labeled cetuximab (2 mg/ml; a kind gift from Dr. S. Kappel, Department of Gynaecology and Obstetrics, Frankfurt/Main, Germany, and Dr. Steinbach, Merck, Darmstadt, Germany) monoclonal antibody (mAb) was used to study the uptake of macromolecules into tumors. Cetuximab was conjugated using SAIVI Alexa Fluor 680 Labeling Kit (Invitrogen). In the animal experiments, concentrated HSA (20% HSA; Octapharma, Lachen, Switzerland or Baxter, Vienna, Austria) was used to increase the plasma COP.

### *Tumor Models*

In the experiments, female NMRI (Naval Medical Research Institute) mice (5-6 weeks, 18-22 g; Harlan Winkelmann, Borchen, Germany) and female non-obese diabetic/severe combined immunodeficient (NOD/SCID) mice (5-6 weeks; 18-22 g; Gades Animal Facility, University of Bergen, Bergen, Norway, and Møllegard, Skensved, Danmark) were subcutaneously (SC) injected on both flanks with $5 \times 10^6$ A431 cells. In other experiments, female Rowett nude rats (180-200 g; Gades Animal Facility, University of Bergen and Harlan Winkelmann) were SC injected in the neck with $1 \times 10^7$ A431 cells. All animal experiments were approved in accordance with the German animal welfare regulations and the guidelines of the Norwegian State Commission for Laboratory Animals. The animals were kept under specific pathogen-free conditions. Sterilized food and tap water were given *ad libitum*. Mice were anesthetized using ketamine/xylazine (100/10 mg/kg, intraperitoneally; Pharmacia, Erlangen, and BayerVital, Leverkusen, Germany) and rats using pentobarbital (60 mg/kg, intraperitoneally; Sigma, Taufkirchen, Germany). All animals were placed on regulated heating pads to keep the body temperature at 37 to 37.5°C during the experiments. After tumor excision, anesthetized animals were killed.

During the experiments, Rowett rats received an IV infusion of 5 ml of 20% HSA, having a COP of 80 mm Hg for 1 hour (84 μl/min) using a clinical perfusor (Braun, Melsungen, Germany). At distinct time points of the infusion, animals received an IV injection of fluorescent dextrans. In contrast, NOD/SCID mice bearing bilateral A431 tumors (>300 $mm^3$) received an IV bolus injection of 500 μl of 20% HSA, 4% HSA (COP, 16 mm Hg), or 0.9% NaCl. Thirty minutes later, the animals were IV injected with 50 μl of Alexa680-coupled dextrans (2.5 mg/ml) or Alexa680-labeled cetuximab (2 mg/ml).

### *Tumor Interstitial Fluid Pressure Measurements*

Tumor interstitial fluid pressure was evaluated as reported previously using the "micropuncture" technique [17]. Tumor interstitial fluid pressure measurements were done every 3 days using sharpened glass capillaries (tip size, 4-10 μm; outer diameter, 1.0 mm; inner diameter, 0.58 mm) inserted in the outermost tumor tissue layers. The glass capillaries were connected to a servocontrolled counterpressure system. The pressure was recorded using a pressure transducer (1280 C; Hewlett Packard, Waltham, MA) connected to an amplifier and recorder (Gould Instruments, Ballainvilliers, France). Glass capillaries were filled with 0.5 M NaCl solution colored with Evans Blue dye (Merck) to visualize the capillary tip. Recording of TIFP started when tumors reached a volume of 500 $mm^3$ or greater. The measurements were performed 0.4 to 0.6 mm inside the tumor tissue using a micromanipulator (Leitz, Wetzlar, Germany) and a stereomicroscope (Wild M5; Leitz) for visual guidance of the glass capillaries. Special care was taken to avoid compression or stretching of tumor tissue during the capillary insertion. Measurements were accepted when the following three criteria were met: 1) an increased feedback gain

did not change the recorded pressure values; 2) suction applied by the servocontrolled pump gave an increased electric resistance in the capillary, verifying an open communication to interstitial fluid pressure because of lower tonicity of the fluid entering the capillary; 3) after the measurement, the zero value in a saline-filled cup placed at the level of micropipette insertion was unchanged compared with the premeasurement value.

### *Colloid Osmotic Pressure Measurements*

Colloid osmotic pressure was analyzed in serum samples using a microcolloid osmometer with membranes with a cutoff size of 30 kDa [18]. A minimum of 0.5 μl of serum was needed to perform the measurement. Usually, samples of 1 to 1.5 μl were applied to the osmometer membrane. All samples were collected at distinct time points before, during, or after the infusion of animals with 20% HSA (Baxter, Unterschleisheim, Germany) or control solutions. Before the start of a new test run, the osmometer was calibrated using PBS solution.

### *Immunofluorescence*

For immunofluorescence studies, tumors were embedded in TissueTek-Medium (Jung, Heidelberg, Germany) and immediately frozen. Frozen samples were cut in thin slides of 8 to 12 μm using a Leica Kryostat (Leica Microsystems, Wetzlar, Germany), placed on object slides, and stored at 4°C in nontransparent boxes to protect fluorescent dyes from bleaching. Sections were examined using an Olympus BX5 fluorescence microscope (Olympus, Hamburg, Germany).

### *Time Domain Optical Imaging*

Time domain optical imaging experiments were performed with an Optix MX2 system (ART, Inc, Saint Laurent, Quebec, Canada) in near-infrared (NIR) configuration. This consisted of a 670-nm pulsed laser diode with a repetition rate of 80 MHz (translating to an acquisition time window of 12.5 nanoseconds) using a PMT detector with a 700-nm long-pass filter. A translational stage and galvanometric mirrors enable raster scanning along *x* and *y* directions, with scanning resolutions of 1 mm used. Briefly, mice were depilated at the region of interest, and background images were acquired under isoflurane anesthesia (1.5% isoflurane) at distinct time points (10-360 minutes) after administration of Alexa680-labeled dextran or cetuximab. Mice were placed on an adjustable stage in the imaging system, where a two-dimensional scanning region and white light image encompassing the area of the mouse were acquired through a top-reviewing digital camera. The samples were then automatically moved into the imaging chamber for scanning. The laser power for each mouse and time point was optimized per sample before scanning. Resultant images were analyzed with Optix Optiview (2.0.01 and 2.01.00) software (ART, Inc).

Conventional whole-body reflectance fluorescence imaging and fluorescence imaging using an epi-illumination or trans-illumination source rely on a high signal-to-background ratio to determine fluorescence accumulation in a target organ. However, quantification or semiquantification of the desired fluorescent signal is frustrated by inability to decouple background fluorescence, animal autofluorescence, and accumulated fluorescence, particularly when using exogenous fluorescent probes. In time domain imaging (Figure 1*A*), using a pulsed laser diode, raster scan (in this instance, 1-mm resolution = fluorescence images of pixel size 1 $mm^2$), and time-correlated detection system, measurement of the fluorescence signal and its decay curve over time per fluorescence image pixel (or raster point) is permitted [19]. Thus, this information can be used to generate the fluorescence decay profile, or fluorescence lifetime, per pixel. Before injection of the contrast reagent, a background scan of the region of interest, including tumor and normal tissues, is generated (Figure 1*B*). Each pixel of the resultant image corresponds to the fluorescence intensity per predetermined raster point and its subsequent fluorescence lifetime. Thus, by cumulating all pixels in the background image, one can determine the distribution of all fluorescence lifetimes and their intensities (generally, autofluorescence) per animal. After administration of NIR imaging probe (Figure 1*C*, demonstrated here for mAb labeled with Alexa680) and subsequent imaging, analysis of the fluorescence image reveals differences in the fluorescence lifetime of normal and tumor tissue pixels. Accordingly, distinct lifetime distributions can be observed for autofluorescence, background fluorescence in normal tissues (consequent of circulating contrast reagent), and tumor-associated fluorescence [20,21]. It has previously been demonstrated that time domain imaging can be used to decouple the specific lifetimes of fluorescent proteins from that of tissue autofluorescence with similar spectral properties [19] and that fluorescence lifetimes of imaging probes are affected by environmental changes such as pH and $[Ca^{2+}]$ [22,23]. By gating for both the fluorescence lifetime and fluorescence intensity range of the specific lifetime distribution of tumor-associated fluorescence, one can exclude autofluorescence and background fluorescence (Figure 1*D*). Ultimately, this method permits the approximation of tumor-associated fluorescence.

## Results

### *Acute Reduction in TIFP Results with Increased Uptake of Dextrans*

Initially, we recorded the increase of TIFP during tumor growth. Using the A431 tumor xenograft model (NMRI mice and *rnu/rnu* rats), we found that TIFP increased uniformly as a function of tumor volume (Figure 2*A*) when measured using the "wick-in-needle" technique at distinct time points ($n$ = 10 tumors per species). Consequently, we evaluated if lowering of TIFP facilitated the uptake of

**Figure 1.** Time domain molecular imaging. (A) Using a 670-nm pulsed laser diode, (1) the subject is irradiated with NIR light resulting in (2) excitation of fluorophore and (3) subsequent detection of fluorescence emission. Each pixel of the resultant image encodes not only the fluorescence intensity but also its fluorescence lifetime. (B) Before injection of fluorescent contrast reagent, background scans are completed, and analysis of fluorescence lifetimes on a per-pixel basis permits determination of the distribution of the animal's endogenous autofluorescence lifetimes. (C) Subsequent injection of contrast reagent (in this instance, fluorescently labeled antibody), imaging, and analysis of fluorescence lifetime distribution reveal two new peaks corresponding to tumor-associated fluorescence and normal tissue-accumulated background fluorescence lifetimes. (D) By gating (fluorescence intensity and lifetime range) for the specific lifetime distribution of interest, an image of tumor-associated fluorescence can be generated to quantify tumoral fluorescence only.

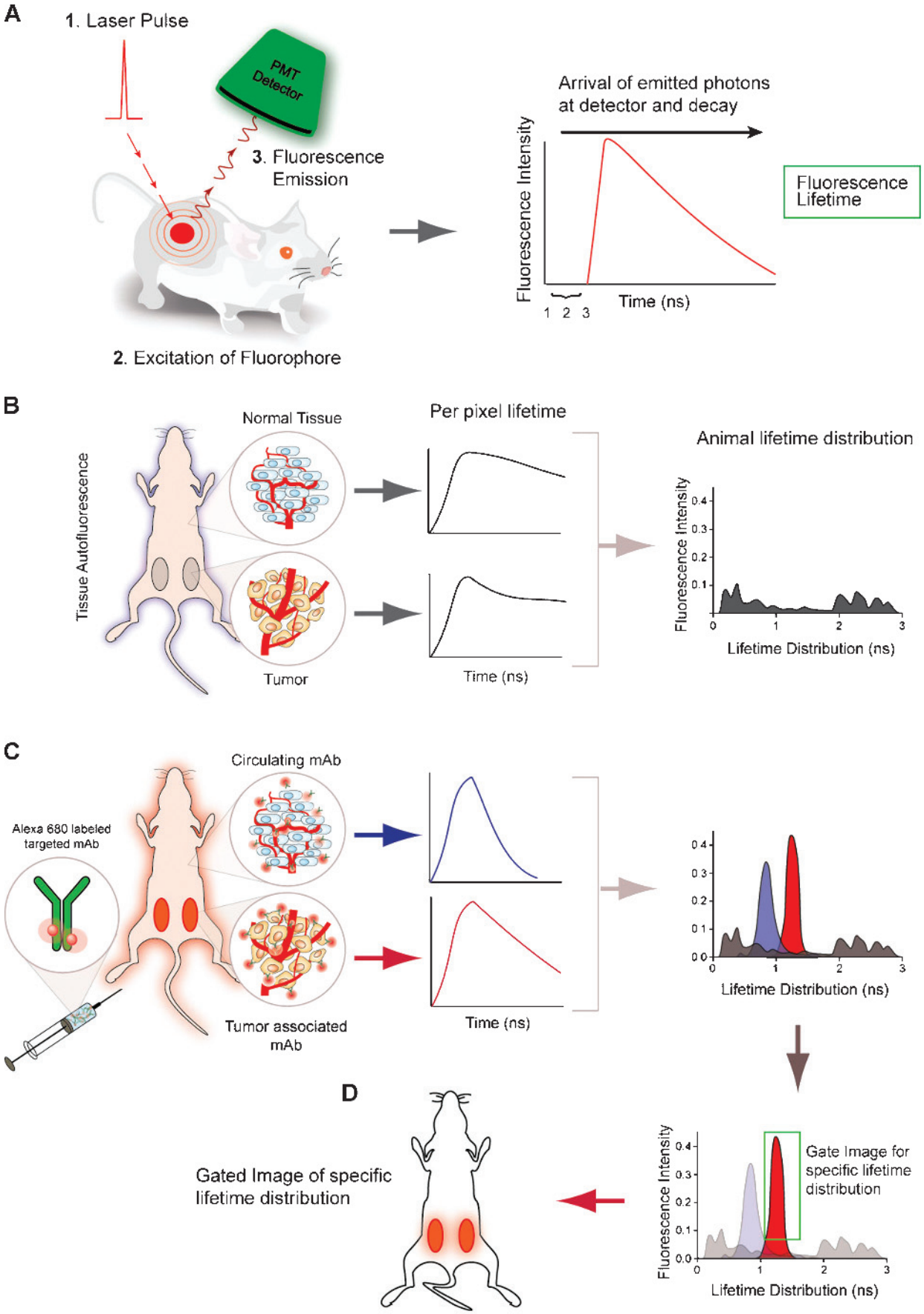
A
1. Laser Pulse
PMT Detector
3. Fluorescence Emission
2. Excitation of Fluorophore
Arrival of emitted photons at detector and decay
Fluorescence Intensity
Time (ns)
1 2 3
Fluorescence Lifetime
B
Normal Tissue
Tissue Autofluorescence
Tumor
Per pixel lifetime
Time (ns)
Animal lifetime distribution
Fluorescence Intensity
Lifetime Distribution (ns)
C
Circulating mAb
Alexa 680 labeled targeted mAb
Tumor associated mAb
Time (ns)
Lifetime Distribution (ns)
D
Gated Image of specific lifetime distribution
Gate Image for specific lifetime distribution
Fluorescence Intensity
Lifetime Distribution (ns)

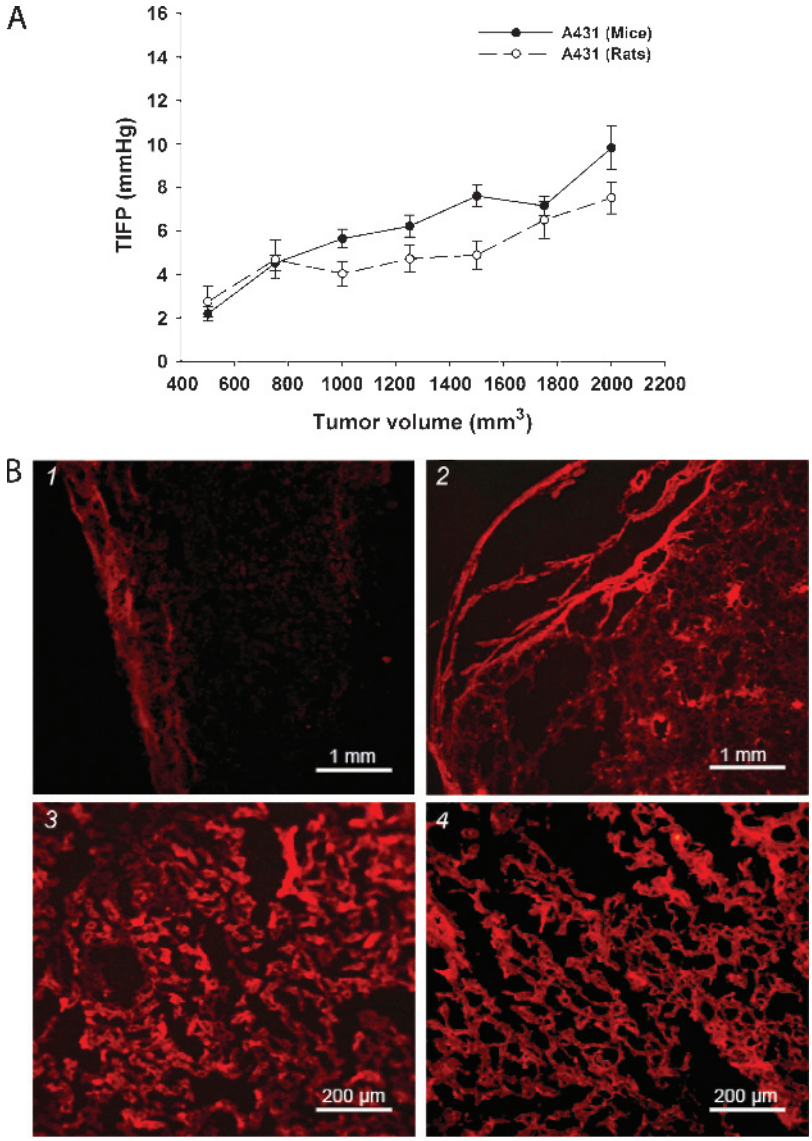


**Figure 2.** Tumor interstitial fluid pressure measurements and the effect of tumor puncture on the uptake of dextrans. (A) Comparison of TIFP values of A431 tumors in NMRI mice and Rowett nude rats. In both animal species, TIFP increased with tumor volume. Data are shown as mean (±SEM) increase of TIFP. $n = 10$ per species. (B) Uptake of TRITC-labeled dextrans in TIFP-lowered A431 tumors and kidney tissue of NMRI mice. A431 tumors were punctured using 20-G needles. Afterwards, mice were injected IV with 50 $\mu$l of fluorescent dextran solutions (2.5 mg/ml). All tissue samples, namely, (1) untreated control tumor, (2) punctured tumor, (3) untreated kidney tissue, and (4) punctured kidney tissue, were excised 30 minutes after the application of the fluorescent dextrans.

macromolecules. Thus, the uptake of IV injected fluorescently labeled dextrans in the tumor interstitial space was determined after lowering of TIFP by tumor puncture, as previously described [14]. As illustrated in Figure 2*B* (*panels 1 and 2*), uptake of dextrans in punctured tumors was significantly enhanced in comparison to untreated control tumors. In other tissues (Figure 2*B*, *panels 3 and 4*), for example, kidney, capsule puncture had no effect on the uptake of labeled dextrans. Although these experiments clearly demonstrated that tumor puncture lowers TIFP and enhances the uptake of macromolecules, such methodology is clinically impracticable.

### *Increased COP in Plasma Increases Tumor Uptake of Dextrans*

Thus, we tested if an increase of the vascular COP by systemically administered HSA would generate a fluid efflux from tumor tissue resulting in a decreased TIFP. Consequently, IV administration of 20% HSA (wt/vol) raised the plasma COP significantly resulting in a TIFP decrease (Figure 3*A*). To examine if this approach was sufficient to significantly increase intratumoral uptake of macromolecules, A431 tumor-bearing rats were infused with 20% HSA followed by IV injection of fluorescently labeled dextrans at distinct time points. It was found that the uptake of dextrans into the tumor interstitium was increased in rats injected between 2 and 3 hours after the HSA application (Figure 3*B*, *panels 3 and 4*) compared with untreated control tumors (Figure 3*B*, *panel 1*) and in rats injected only 30 minutes after the HSA application (Figure 3*B*, *panel 2*).

### *Increased Tumor Uptake of Macromolecules Can Be Visualized by Time Domain Fluorescence Imaging*

To semiquantify this uptake *in vivo*, we used a novel time domain fluorescence imaging modality to specifically quantify fluorescence

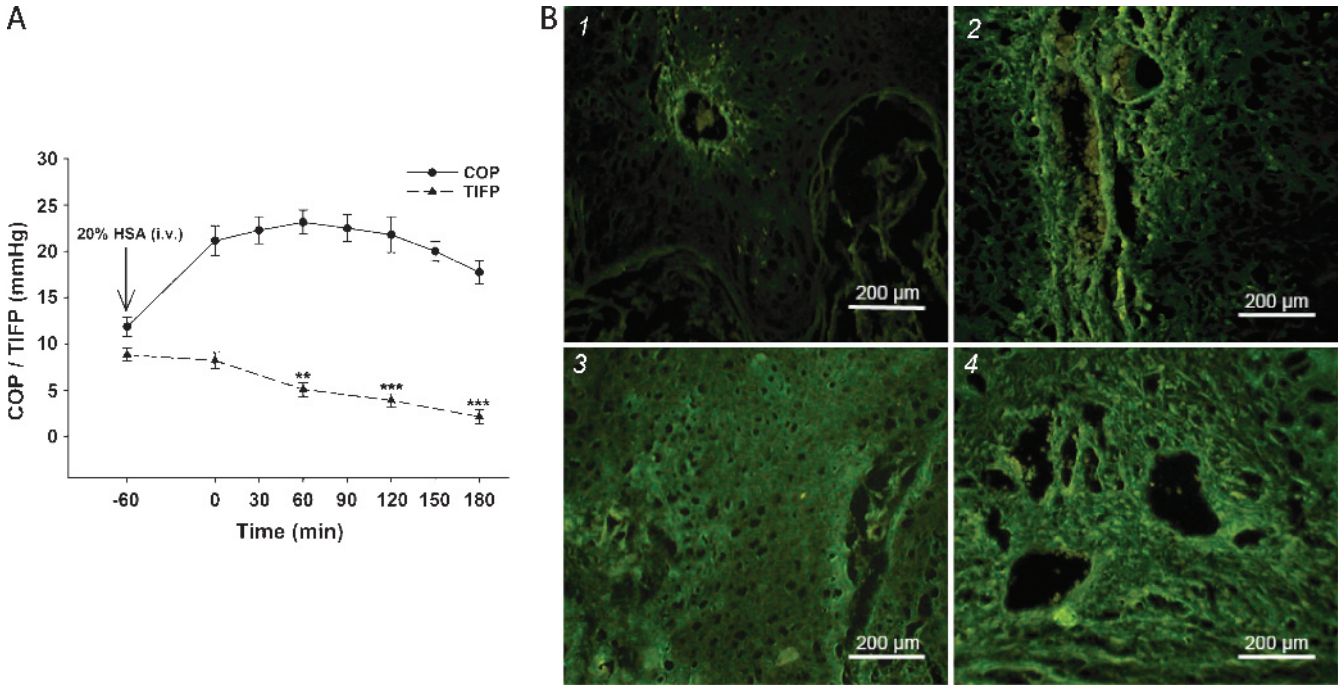


**Figure 3.** Tumor interstitial fluid pressure reduction through concentrated HSA and subsequent effects on the uptake of macromolecules. (A) Intravenous injection of 20% HSA significantly increased the plasma COP in Rowett nude rats. The COP rise correlated with a significant lowering of TIFP after the injection of 20% HSA. (B) Uptake of Alexa488-coupled dextrans (10 kDa) in A431 tumors at distinct time points after an IV injection of 20% HSA. (1) Untreated control tumor (no HSA injection), (2) dextran injection 1 hour after the HSA injection, (3) dextran injection 2 hours after the HSA injection, and (4) dextran injection 3 hours after the HSA injection. Tissue slides were prepared according to the description in Figure 2*B*.

the accumulated fluorescent dextran in A431 tumors. NOD/SCID mice bearing SC A431 tumors were pretreated with 0.9% NaCl solution as volume control, low-concentration HSA (4%) control, or 20% HSA, 30 minutes before injection of dextran labeled with Alexa680 and imaged for 6 hours. Resultant images (Figure 4*A*) were gated for fluorescence lifetimes of accumulated tumoral fluorescence (Figure 4*B*) from circulating fluorescence or exogenous autofluorescence, facilitating distinction of tumoral-only accumulated fluorescence (Figure 4*A*, *third picture*). Subsequently, no difference in tumoral accumulated fluorescence was observed between the NaCl and 4% HSA groups. In contrast, the injection of 20% HSA facilitated a significant uptake and delayed intratumoral dextran clearance (Figure 4*C*), demonstrating that enhanced uptake of macromolecules is HSA concentration–dependent. Of note, the intratumoral uptake of dextrans was increased approximately 95% in mice that were treated with 20% HSA for 30 minutes (Figure 4*D*). Interspecies differences were observed in dextran uptake kinetics between mice and rats; however, in both species, the injection of 20% HSA led to considerably increased uptake of macromolecules.

### *Infusion of Hyperoncotic HSA Results in Increased Accumulation of Therapeutic Antibodies*

We demonstrated the therapeutic applicability of this concept conjugating the clinically used mAb cetuximab (Erbitux) to Alexa680 and monitored its accumulation after preinjection (30 minutes) of 20% HSA or control vehicles. Time domain imaging and gating for the fluorescent lifetime of tumoral cetuximab–Alexa680 fluorescence (Figure 5*A*) again demonstrated significantly increased uptake of cetuximab in A431 tumors after 20% HSA treatment in comparison to controls (Figure 5*B*).

### *Injection of Cetuximab after 20% HSA Infusion Delays Tumor Growth After Stopping Cetuximab Treatment*

Finally, to demonstrate the physiological effect on tumor growth, A431 tumor-bearing NMRI mice were treated with cetuximab (2 mg/ml) 30 minutes after injection of 20% HSA, 4% HSA, or 0.9% NaCl (500 µl each) twice weekly. Control animals received only 0.9% NaCl injections (500 µl) twice weekly. As expected, tumor growth in control mice was significantly augmented compared with cetuximab-treated animals. Control animals were withdrawn from the experiment at day 20 owing to large tumor volumes. No significant differences in tumor growth were detected between all cetuximab-treated groups until cetuximab application was stopped on day 30. Afterward, mice treated with 20% HSA plus cetuximab continued tumor regression. In contrast, a significant progression in A431 tumor growth was measured in all other treatment groups (Figure 6*A*). Furthermore, evaluation of blood pressure alterations after IV injection of 4% HSA, 20% HSA, or 0.9% NaCl in NMRI mice was performed through intra-arterial blood pressure measurement for 3 hours. Although no effect on blood pressure was observed in response to 4% HSA or 0.9% NaCl, treatment with 20% HSA caused a significant increase in blood pressure just 1 hour after IV injection (Figure 6*B*), which approached control levels after 3 hours. To prove the effectiveness of cetuximab in reducing tumor cell growth, A431 cells were incubated *in vitro* for 1 hour with different concentrations of cetuximab. Cells were analyzed for phospho-p44/42 by Western blot analysis. It was

found that cetuximab diminishes phosphorylation of the proliferation-associated mitogen-activated protein kinase p44/42 at concentration levels of 5 to 10 μg completely (Figure 6*C*).

## Discussion

An increased TIFP leads to a reduced convectional-driven transendothelial fluid transport with clinical and therapeutic implications. Particularly, the transport and uptake of therapeutic drugs [12] are hampered, contributing to a lowered retention time of chemotherapeutics within the tumor tissue [24,25]. In this respect, therapeutic strategies enabling TIFP lowering may enhance the efficacy of antitumor drugs [5]. It has been demonstrated that TIFP can be lowered by local peritumoral application of prostaglandin $E_1$ or hyaluronidase [26,27]. Both treatment options feature the disadvantage that they are limited solely to externally accessible tumors and cannot be applied in a systemic treatment.

Here, we pursued a new approach to lower the TIFP, increase the uptake of macromolecules into tumor tissue, and study the effect of an increased COP on TIFP and the uptake of macromolecules. Initially, TIFP in A431 tumors of immunosuppressed mice and rats was measured and related to tumor volume. In particular, A431 tumors suggested a strong correlation between TIFP and tumor volume. These results are in concert with published data showing that TIFP increases with the tumor volume in other tumor species [28–30]. A431 tumors were punctured followed by IV injection of fluorescently labeled dextrans to check if lowering of TIFP increases the uptake of macromolecular substances. As a result of tumor puncture, an increased uptake of dextrans was detected in comparison to untreated tumors or punctured control tissues (e.g., kidney). Nevertheless, the use of the puncture method to lower TIFP is strictly limited to externally accessible tumors and may not be transferred into the clinic. Having demonstrated that reduced TIFP facilitates the uptake of macromolecules, we investigated the effect of an increased COP on the TIFP and consequent uptake of fluorescent-labeled macromolecules. We confirmed that IV injection of 20% HSA resulted in a significant reduction of TIFP in immunosuppressed mice and rats. Concurrently, the systemic blood pressure rose moderately for a short period before dropping toward base levels. Furthermore, improved delivery of IV administered fluorescently labeled dextrans or fluorescently labeled cetuximab to tumors was achieved through the decrease of TIFP, with accumulation quantified by a novel time domain molecular imaging.

The rationale for our new proposed therapy is that the high plasma COP results in fluid mobilization from the tumor interstitium (as well as other tissues) to the plasma. That this is actually occurring is shown by the observed TIFP reduction and the concomitant increase in blood pressure. Despite net bulk flow of fluid from tumor

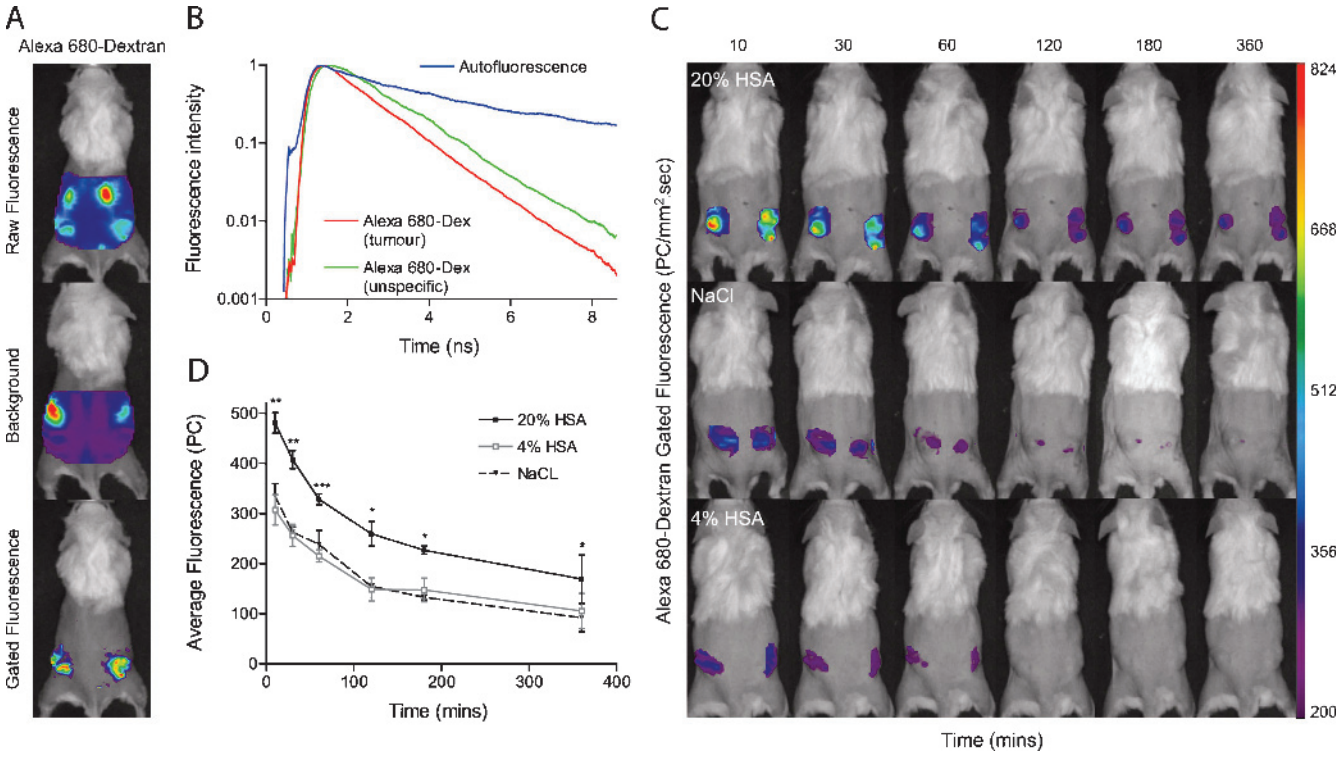


**Figure 4.** Time domain fluorescence imaging of Alexa680-conjugated dextran accumulation 30 minutes after the IV injection of 20% HSA. NOD/SCID mice bearing bilateral A431 tumors (>300 $mm^3$) received an IV bolus injection of 500 μl of 20% HSA, 4% HSA, or 0.9% NaCl ($n = 6$ per group). Thirty minutes later, the animals were IV injected with 50 μl of Alexa680-coupled dextrans. (A) Background and raw fluorescence images were acquired before and after Alexa680-dextran injection. Raw fluorescence images of Alexa680-dextran chromophor (first picture), with predominant circulation, and filtration through the kidneys, coupled with autofluorescence (as depicted in the background scan, second picture), made it impossible to distinguish and quantify accumulated tumoral fluorescence. (B) Gating for the fluorescence lifetime of tumor-accumulated Alexa680-dextran revealed specifically accumulated Alexa680-dextran in tumors (depicted in third picture of panel A). (C) Representatives of each group illustrated. (D) Average photon counts (±SEM) were plotted *versus* time for Alexa680-dextran tumor-accumulated fluorescence, where $*P < .05$, $**P < .01$, $***P < .001$. *PC* indicates photon counts.

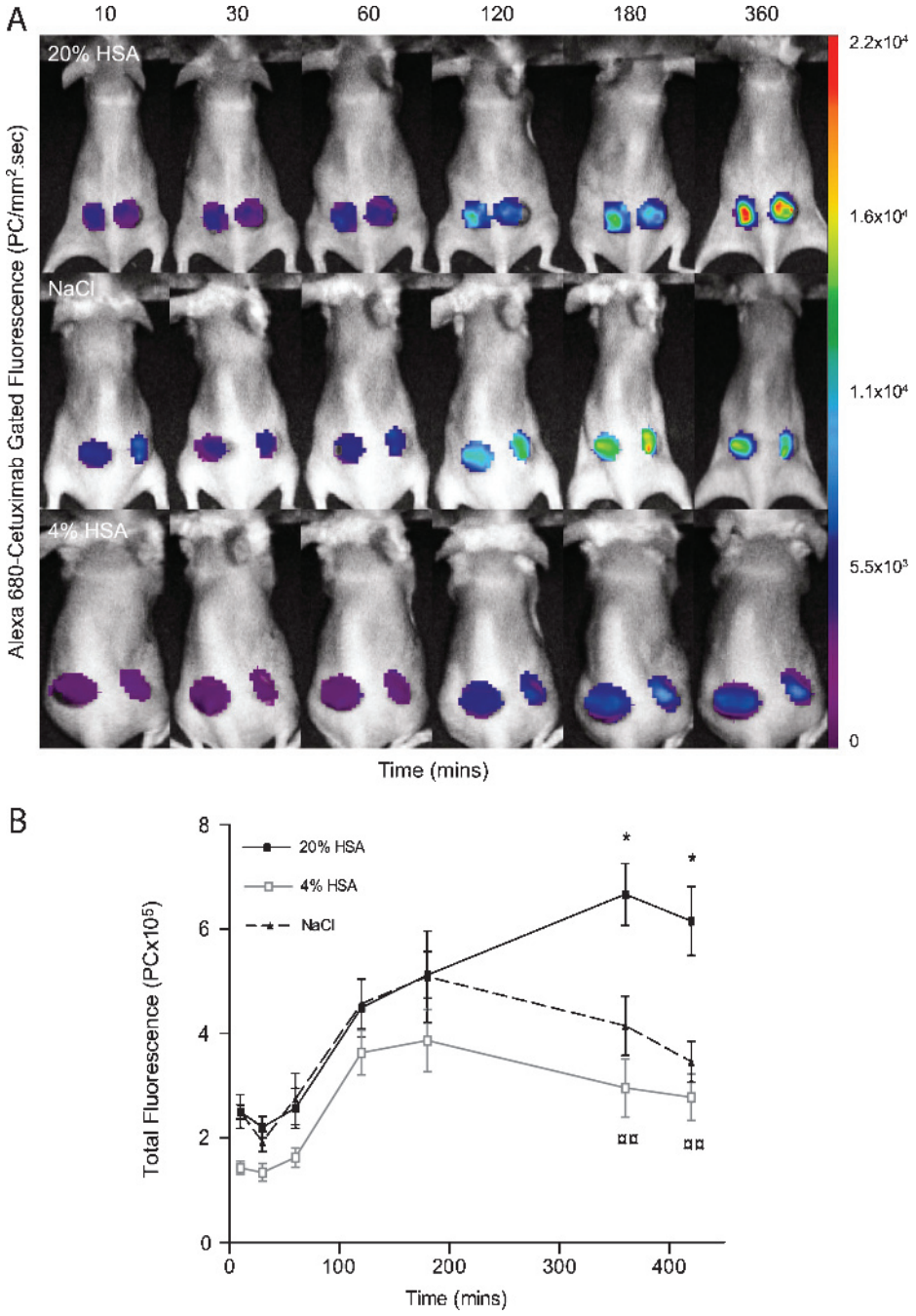


**Figure 5.** Time domain fluorescence imaging of Alexa680-conjugated cetuximab accumulation 30 minutes after the IV injection of 20% HSA. (A) NOD/SCID mice bearing bilateral A431 tumors ($n = 4$; 300 $mm^3$) were treated with cetuximab-Alexa680 (2 mg/ml) 30 minutes after injection of 20% HSA, 4% HSA, or 0.9% NaCl (500 $\mu$l each), imaged by time domain fluorescence imaging (10-360 minutes) and raw data gated for tumor-accumulated fluorescence lifetime of cetuximab-Alexa680 (1.5 nanoseconds). Representative images of each group are depicted. (B) Graphical presentation of cetuximab-Alexa680 bound fluorescence (total photon counts ± SEM) *versus* time for all tumors per treatment arm. *$P < .05$. *PC* indicates photon counts.

to plasma, macromolecules are transported in the opposite direction as evidenced by the increased uptake. This apparent paradox may be explained if we consider the sequence of effects evidenced by the ensuing change in blood pressure and plasma COP and that the macromolecule in question (i.e., macromolecular dextran or mAb, in the present context called tracer) is transported by bulk flow as well as diffusion. Furthermore, the well-known heterogeneity of tumor perfusion pattern and the tumor interstitium *per se* may also have an influence. The initial rise in COP in plasma will mobilize tracer-free interstitial fluid to plasma, again resulting in increased blood and capillary pressure and filtration of tracer-containing fluid into the interstitium. Such fluid mobilization occurs despite leaky vessels having a high capillary permeability and a low osmotic reflection coefficient, $\sigma$, in tumors (reviewed in [6,9]) and may be even higher in normal tissues, such as muscle, having $\sigma$ close to 1.0 [6]. In addition, the increased capillary pressure and reduced IFP induced by the hyperoncotic solution

will most likely result in perfusion of previously unperfused regions, thus increasing the surface area available for diffusion. Accordingly, diffusion as well as bulk flow works in the same direction and contributes to the observed increased tracer uptake in the tumor.

If the proposed therapy were applied in a clinical situation, the concurrent rise in systemic blood pressure may be a reason for concern. We believe that such an effect would have been modest. Firstly, the effect was moderate and temporary despite infusion of a strongly hyperoncotic solution and the tendency to return to control levels at 180 minutes into the therapy. Furthermore, mobilization of fluid to plasma and a rise in systemic blood pressure will result in a pressure natriuresis and fluid excretion tending to normalize blood pressure in individuals with normally functioning kidneys [31]. Clearly, this potential problem has to be evaluated carefully in a clinical situation.

Although both test substances accumulate in the tumor after treatment with 20% HSA, our data presume a different kinetic between

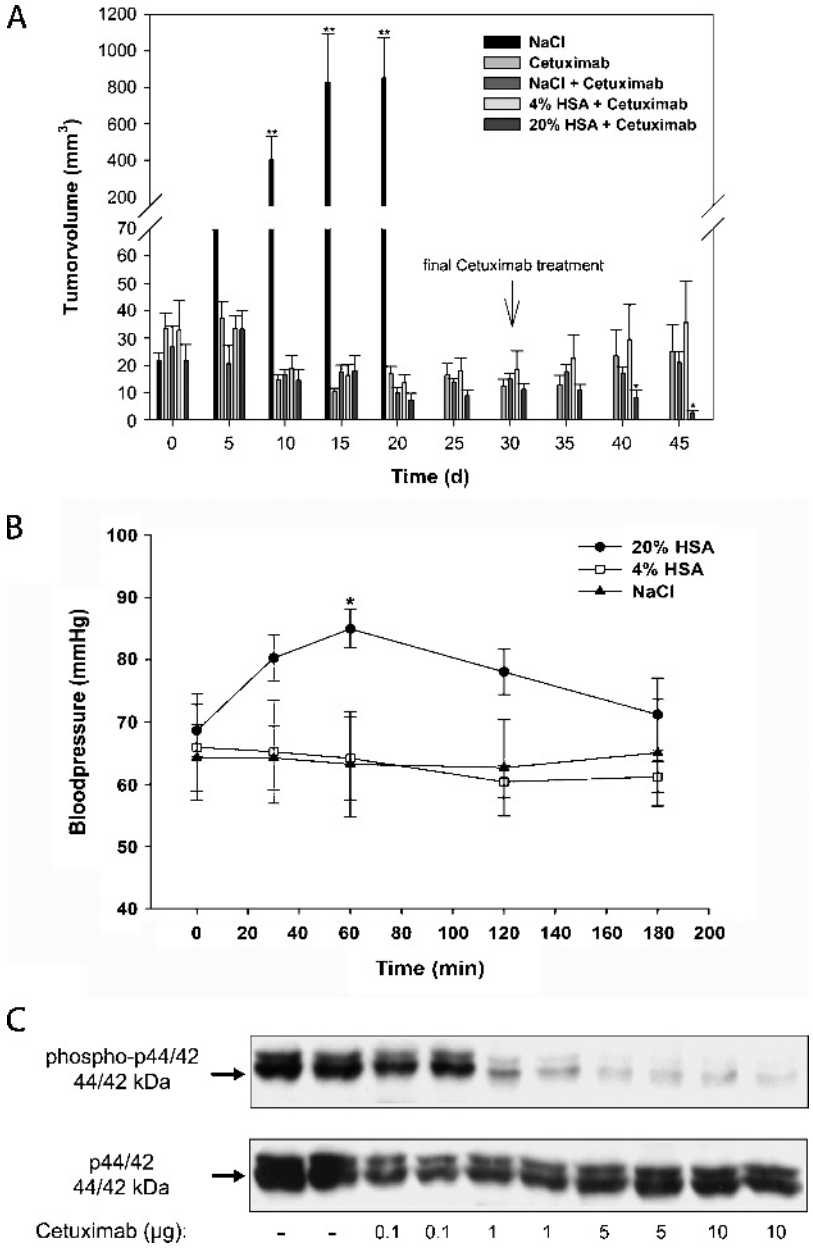


**Figure 6.** Increased COP facilitates the delivery of cetuximab and reduces tumor growth *in vivo*. (A) NMRI nude mice bearing bilateral A431 tumors ($n = 6$ per treatment group; 300 $mm^3$) were treated with cetuximab (2 mg/ml) 30 minutes after injection of 20% HSA, 4% HSA, or 0.9% NaCl (500 $\mu$l each) twice weekly. Control animals received only 0.9% NaCl injections (500 $\mu$l each) twice weekly. Tumor growth was measured every 5 days. At day 30, cetuximab treatment was stopped at all treatment groups, and animals were followed for tumor growth. Data are shown as mean ± SEM for $n = 6$ tumors per group. *$P < .05$ (20% HSA plus cetuximab *vs* all other cetuximab groups), **$P < .001$ (control *vs* all other groups). (B) Arterial blood pressure was measured continuously from 0 minute before and 180 minutes after the IV injection of 500 $\mu$l of 20% HSA, 4% HSA, or 0.9% NaCl. Data are shown as mean ± SEM for $n = 4$ mice per group. *$P < .05$. (C) *In vitro* incubation of A431 cells with cetuximab inhibits the phosphorylation of the proliferation-associated mitogen-activated protein kinase p44/42-1/2 in a concentration-dependent manner.

dextrans and cetuximab. Dextrans accumulate rapidly followed by a gradual washout. In contrast, cetuximab accumulates slower, but the retention time was markedly prolonged. It seems likely that dextrans, because of their inert chemical character, do not bind to any structure within the tumor and, therefore, show a fast clearance rate. Cetuximab accumulates over time because of its high affinity toward the epidermal growth factor receptor which is overexpressed on A431 tumor cells [32]. In comparison to dextrans, the uptake of cetuximab into the tumor interstitium is delayed because of its higher molecular weight (151.8 *vs* 40 kDa for dextrans).

Experimental data suggest that antagonists against vascular endothelial growth factor (e.g., bevacizumab) and platelet-derived growth factor receptor (e.g., imatinib) also have some lowering effect on TIFP [33,34]. It is assumed that bevacizumab, as a vascular endothelial growth factor antibody, normalizes the tumor vasculature and, therefore, lowers the TIFP. In the case of imatinib, the decreased TIFP is attributed to a reduced contractility of fibroblasts residing in the tumor extracellular matrix [34]. Although both substances given solely only have marginal effects on tumor growth, a combination with classic chemotherapeutics such as 5-fluorouracil or dacarbazine has shown some benefit [35,36]. It seems likely that this improvement is due to the enhanced transvascular transport followed by the TIFP reduction [37–40]. However, the TIFP-lowering effect does not appear immediately after substance application and implies a long-term remodeling of the tumor physiology, for example, tumor vasculature or tumor extracellular matrix [35,41,42]. Therefore, it is difficult to predict the maximum effect on TIFP reduction, which is optimal for the application of chemotherapeutics.

The use of HSA, which interferes with the TIFP on a biophysical level, enables a timely lowering of the TIFP and, therefore, allows establishment of distinct application protocols for antitumor drugs. In conclusion, our data show for the first time that an increased plasma COP lowers the TIFP. Moreover, it was shown that lowering of TIFP enhances delivery and accumulation of macromolecules into solid tumors and delays the tumor growth in the herein used animal model. Thus, the present work proposes a strategic lowering of TIFP through an increased plasma COP that may enhance the clinical efficacy of antitumor therapies.

## Acknowledgments

The authors thank Maike Schultz (Department of Dermatology, Goethe-University, Frankfurt/Main, Germany), Gerd Signe Salvesen (Department of Biomedicine, University of Bergen, Bergen, Norway), and Maren Boge and Kjetil Jacobson (Institute of Medicine, Haematology Section, University of Bergen, Bergen, Norway) for excellent technical assistance.

## References

[1] Jain RK (2001). Delivery of molecular medicine to solid tumors: lessons from *in vivo* imaging of gene expression and function. *J Control Release* **74**, 7–25.

[2] Young JS, Lumsden CE, and Stalker AL (1950). The significance of the tissue pressure of normal testicular and of neoplastic (Brown-Pearce carcinoma) tissue in rabbit. *J Pathol Bacteriol* **62**, 313–333.

[3] Wiig H, Tveit E, Hultborn R, Reed RK, and Weiss L (1982). Interstitial fluid pressure in DMBA-induced rat mammary tumours. *Scan J Clin Lab Invest* **42**, 159–164.

[4] Jain RK and Gerlowski LE (1986). Extravascular transport in normal and tumor tissues. *Crit Rev Oncol Hematol* **5**, 115–170.

[5] Heldin CH, Rubin K, Pietras K, and Östman A (2004). High interstitial fluid pressure—an obstacle in cancer therapy. *Nat Rev Cancer* **4**, 806–813.

[6] Jain RK (1987). Transport of molecules across tumor vasculature. *Cancer Metastasis Rev* **6**, 559–593.

[7] Jain RK (1987). Transport of molecules in the tumor interstitium: a review. *Cancer Res* **47**, 3039–3051.

[8] Tufto I and Rofstad EK (1999). Interstitial fluid pressure and capillary diameter distribution in human melanoma xenografts. *Microvasc Res* **58**, 205–214.

[9] Carmeliet P and Jain RK (2000). Angiogenesis in cancer and other diseases. *Nature* **407**, 249–257.

[10] Leu AJ, Berk DA, Lymboussaki A, Alitalo K, and Jain RK (2000). Absence of functional lymphatics within a murine sarcoma: a molecular and functional evaluation. *Cancer Res* **60**, 4324–4327.

[11] Baxter LT and Jain RK (1989). Transport of fluid and macromolecules in tumors. I. Role of interstitial pressure and convection. *Microvasc Res* **37**, 77–104.

[12] Jain RK (1998). The next frontier of molecular medicine: delivery of therapeutics. *Nat Med* **4**, 655–657.

[13] Hofmann M, Guschel M, Bernd A, Bereiter-Hahn J, Kaufmann R, Tandi C, Wiig H, and Kippenberger S (2006). Lowering of tumor interstitial fluid pressure reduces tumor cell proliferation in a xenograft tumor model. *Neoplasia* **8**, 89–95.

[14] Hofmann M, Schultz M, Bernd A, Bereiter-Hahn J, Kaufmann R, and Kippenberger S (2007). Long-term lowering of tumor interstitial fluid pressure reduces Ki-67 expression. *J Biomech* **40**, 2324–2329.

[15] Starling EH (1896). On absorption of fluids from connective tissue spaces. *J Physiol* **19**, 312–326.

[16] Wiig H, Aukland K, and Tenstad O (2003). Isolation of interstitial fluid from rat mammary tumors by a centrifugation method. *Am J Physiol Heart Circ Physiol* **284**, H416–H424.

[17] Wiig H, Reed RK, and Aukland K (1981). Micropuncture measurement of interstitial fluid pressure in rat subcutis and skeletal muscle: comparison to wick-in-needle technique. *Microvasc Res* **21**, 308–319.

[18] Wiig H, Halleland EG, Fjaertoft M, and Aukland K (1988). Measurement of colloid osmotic pressure in submicrolitre samples. *Acta Physiol Scand* **132**, 445–452.

[19] McCormack E, Micklem DR, Pindard LE, Silden E, Gallant P, Belenkov A, Lorens JB, and Gjertsen BT (2007). *In vivo* optical imaging of acute myeloid leukemia by green fluorescence protein: time-domain autofluorescence decoupling, fluorophore quantification, and localization. *Mol Imaging* **6**, 193–204.

[20] Alves F, Dullin C, Napp J, Missbach-Guentner J, Jannasch K, Mathejczyk J, Pardo LA, Stühmer W, and Tietze LF (2009). Concept of a selective tumour therapy and its evaluation by near-infrared fluorescence imaging and flat-panel volume computed tomography in mice. *Eur J Radiol* **70**, 286–293.

[21] Christian NA, Benencia F, Milone MC, Li G, Frail PR, Therien MJ, Coukos G, and Hammer DA (2009). *In vivo* dendritic cell tracking using fluorescence lifetime imaging and near-infrared–emissive polymersomes. *Mol Imaging Biol* **11**, 167–177.

[22] Lakowicz JR, Szmacinski H, Nowaczyk K, and Johnson ML (1992). Fluorescence lifetime imaging of calcium using Quin-2. *Cell Calcium* **13**, 131–147.

[23] Szmacinski H and Lakowicz JR (1993). Optical measurements of pH using fluorescence lifetimes and phase-modulation fluorometry. *Anal Chem* **65**, 1668–1674.

[24] Boucher Y and Jain RK (1992). Microvascular pressure is the principal driving force for interstitial hypertension in solid tumors: implications for vascular collapse. *Cancer Res* **52**, 5110–5114.

[25] Lee I, Boucher Y, Demhartner TJ, and Jain RK (1994). Changes in tumour blood flow, oxgenation and interstitial fluid pressure induced by pentoxifylline. *Br J Cancer* **69**, 492–496.

[26] Brekken C and De Lange Davies C (1998). Hyaluronidase reduces the interstitial fluid pressure in solid tumours in a non-linear concentration–dependent manner. *Cancer Lett* **131**, 65–70.

[27] Salnikov A, Iversen VV, Koisti M, Sundberg C, Johansson L, Stuhr LB, Sjöquist M, Ahlström H, Reed RK, and Rubin K (2003). Lowering of tumor interstitial fluid pressure specifically augments efficacy of chemotherapy. *FASEB J* **17**, 1756–1758.

[28] Boucher Y, Kirkwood JM, Opacic D, Desantis M, and Jain RK (1991). Interstitial hypertension in superficial metastatic melanomas in humans. *Cancer Res* **50**, 6691–6694.

[29] Gutmann R, Leunig M, Feyh J, Goetz AE, Messmer K, Kastenbauer E, and Jain RK (1992). Interstitial hypertension in head and neck tumors in patients: correlation with tumor size. *Cancer Res* **52**, 1993–1995.

[30] Nathanson SD and Nelson L (1994). Interstitial fluid pressure in breast cancer, benign breast conditions, and breast parenchyma. *Ann Surg Oncol* **1**, 333–338.

[31] Guyton and Hall (2005). *Textbook of Medical Physiology*, 11th ed., Elsevier Ltd, Oxford, UK.

[32] Solbach C, Sterner-Kock A, Roller M, Schnürch HG, Stegmüller M, Caspar-Bell G, Schumm-Draeger PM, Kaufmann M, and Knecht R (2002). Antitumor effect of Mab EMD 55900 depends on EGF-R expression and histopathology. *Neoplasia* **4**, 237–242.

[33] Lee CG, Heijn M, Di Tomaso E, Griffon-Etienne C, Ankukiewicz M, Koike C, Park KR, Ferrara N, Jain RK, Suit HD, et al. (2000). Anti-vascular endothelial growth factor treatment augments tumor radiation response under normoxic or hypoxic conditions. *Cancer Res* **60**, 5565–5570.

[34] Pietras K, Östmann A, Sjöquist M, Buchdunger E, Reed RK, Heldin CH, and Rubin K (2001). Inhibition of platelet-derived growth factor receptors reduces interstitial hypertension and increases transcapillary transport in tumors. *Cancer Res* **61**, 2929–2934.

[35] Willett CG, Boucher Y, Di Tomaso E, Duda DG, Munn LL, Tong RT, Chung DC, Sahani DV, Kalva SP, Kozin SV, et al. (2004). Direct evidence that the VEGF-specific antibody bevacizumab has antivascular effects in human rectal cancer. *Nat Med* **10**, 145–147.

[36] Ogawa Y, Kawamura T, Furuhashi M, Tsukamoto K, and Shimada S (2008). Improving chemotherapeutic drug penetration in melanoma by imatinib mesylate. *J Dermatol Sci* **51**, 190–199.

[37] Inai T, Mancuso M, Hahizume H, Baffert F, Haskell A, Baluk P, Hu-Lowe DD, Shalinsky DR, Thurston G, Yancopoulos GD, et al. (2004). Inhibition of vascular endothelial growth factor (VEGF) signaling in cancer causes loss of endothelial fenestrations, regression of tumor vessels, and appearance of basement membrane ghosts. *Am J Pathol* **165**, 35–52.

[38] Tong RT, Boucher Y, Kozin SV, Winkler F, Hicklin DJ, and Jain RK (2004). Vascular normalization by vascular endothelial growth factor receptor 2 blockade induces a pressure gradient across the vasculature and improves drug penetration in tumors. *Cancer Res* **64**, 3731–3736.

[39] Pietras K, Rubin K, Sjöblom T, Buchdunger E, Sjöquist M, Heldin C-H, and Östman A (2002). Inhibition of PDGF receptor signaling in tumor stroma enhances antitumor effect of chemotherapy. *Cancer Res* **62**, 5476–5484.

[40] Pietras K (2004). Increasing tumor uptake of anticancer drugs with imatinib. *Semin Oncol* **31**, 18–23.

[41] Baranowska-Kortylewicz J, Abe M, Pietras K, Kortylewicz ZP, Kurizaki T, Nearman J, Paulsson J, Mosley RL, Enke CA, and Östman A (2005). Effect of platelet-derived growth factor receptor-β inhibition with STI571 on radioimmunotherapy. *Cancer Res* **65**, 7824–7831.

[42] Vlahovic G, Rabbani ZN, Herndon I, Dewhirstz MW, and Vujaskovic Z (2006). Treatment with imatinib in NSCLC is associated with the decrease of phosphorylated PDGFR-β and VEGF expression, decrease in interstitial fluid pressure and improvement of oxygenation. *Br J Cancer* **95**, 1013–1019.